Eur. Phys. J. C 38, 475–482 (2005)
Digital Object Identifier (DOI) 10.1140/epjc/s2004-02059-0

THE EUROPEAN PHYSICAL JOURNAL C

Diffractive $\gamma\gamma$ production at hadron colliders

V.A. Khoze[1,2,a], A.D. Martin[1], M.G. Ryskin[1,2], W.J. Stirling[1,3]

[1] Department of Physics and Institute for Particle Physics Phenomenology, University of Durham, DH1 3LE, UK
[2] Petersburg Nuclear Physics Institute, Gatchina, St. Petersburg, 188300, Russia
[3] Department of Mathematical Sciences, University of Durham, DH1 3LE, UK

Received: 10 September 2004 / Revised version: 8 October 2004 /
Published online: 1 December 2004 –

Abstract. We compute the cross section for exclusive double-diffractive $\gamma\gamma$ production at the Tevatron, $p\bar{p} \to p + \gamma\gamma + \bar{p}$, and the LHC. We evaluate both the gg and $q\bar{q}$ t-channel exchange contributions to the process. The observation of exclusive $\gamma\gamma$ production at the Tevatron will provide a check on the model predictions and offer an opportunity to confirm the expectations for exclusive double-diffractive Higgs production at the LHC.

1 Introduction

The experimental study of the central exclusive double-diffractive production processes at the Tevatron is interesting in its own right, since it is an ideal way to improve our understanding of diffractive processes and the dynamics of the pomeron exchange. Moreover such observations can provide a valuable check of the theoretical models and experimental methods which may be used to search for new physics at LHC [2]. Of particular interest is exclusive Higgs boson production, $pp \to p + H + p$ [7]. The + signs are used to denote the presence of large rapidity gaps; here we will simply describe such processes as "exclusive", with "double-diffractive" production being implied. The predictions for exclusive production are obtained by calculating the diagram of Fig. 1 using perturbative QCD. In addition we have to calculate the probability that the rapidity gaps are not populated by secondaries from the underlying event.

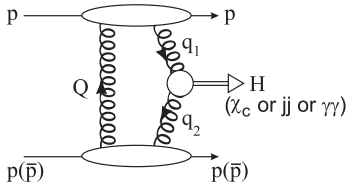

Fig. 1. Schematic diagram for exclusive Higgs production at the LHC, $pp \to p + H + p$. The exclusive production of the states shown in the brackets are possible "standard candles", where the model predictions may, in principle, be checked by measurements at the Tevatron. Here we are concerned with the last process, $p\bar{p} \to p + \gamma\gamma + \bar{p}$. Predictions already exist for the exclusive production of Higgs bosons [1–3], χ_c,χ_b [4,5] and dijets [1,2,6]

[a] e-mail: V.A.Khoze@durham.ac.uk

However it is not easy to find an exclusive process which may be observed at the Tevatron and so act as a "standard candle" for the theoretical predictions for exclusive Higgs production. Let us consider the possibilities. These are shown in brackets in Fig. 1.

Recently the first "preliminary" result on exclusive χ_c production has been reported [8]. Although it is consistent with perturbative QCD expectations [4,5], the mass of the χ_c boson, which drives the scale of the process, is too low to justify just the use of perturbative QCD[1].

One possible process with a larger scale is the exclusive production of a pair of high E_T jets, $p\bar{p} \to p+jj+\bar{p}$ [1,2,6]. In principle, this process appears to be an ideal "standard candle". The expected cross section is rather large, and we can study its behaviour as a function of the mass of the dijet system. Unfortunately in the present CDF environment, the background from the "inelastic pomeron–pomeron collisions" contribution is large as well. Theoretically the exclusive dijets should be observed as a narrow peak, sitting well above the background, in the distribution of the ratio

$$R_{jj} = E_{\rm dijet}/E_{PP} \qquad (1)$$

at $R_{jj} = 1$, where E_{PP} is the energy of the incoming pomeron–pomeron system. In practice the peak is smeared out due to hadronisation and the jet-searching algorithm. For jets with $E_T = 10\,\text{GeV}$ and a jet cone $R < 0.7$, more than 1 GeV will be lost outside the cone, leading to
(i) a decrease of the measured jet energy of about 1–2 GeV[2],

[1] Even lower scales correspond to the fixed-target central double-diffractive meson resonance production observed by the WA102 collaboration at CERN [9]. Therefore, it is intriguing that the qualitative features of the observed p_t and azimuthal angular distributions appear to be in good agreement with the perturbatively based expectations [10].

[2] Note that the jet E_T were not corrected in the preliminary data presented in [8,11].

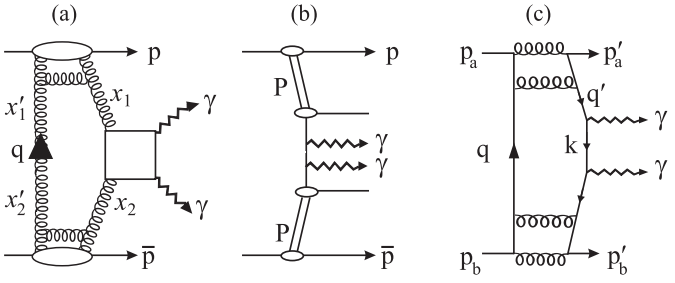

Fig. 2. a Exclusive $\gamma\gamma$ production driven by two-gluon t-channel exchange, and the backgrounds arising from **b** $\gamma\gamma$ produced in a pomeron–pomeron initiated subprocess, accompanied by soft undetected hadrons and **c** from $\gamma\gamma$ production via t-channel quark–antiquark exchange. All permutations of the particle lines are implied

and
(ii) a rather wide peak ($\Delta R_{jj} \sim \pm 0.1$) in the R_{jj} distribution. The estimates based on [2] give an exclusive cross section for dijet production with $E_{\rm T} > 25\,{\rm GeV}$ (and CDF cuts) of about 40 pb, which is very close to the recent CDF measurement [8, 11],

$$\sigma(R_{jj} > 0.8,\ E_{\rm T} > 25\,{\rm GeV}) = 34\ \pm 5({\rm stat})\ \pm 10({\rm syst})\,{\rm pb}\,. \quad (2)$$

Bearing in mind the large uncertainties (in both the theoretical calculations and in experimental identification of low $E_{\rm T}$ jets) at low scales, the predictions [2, 12] for $E_{\rm T} > 7, 10\,{\rm GeV}$ are also in agreement with the corresponding CDF measurements [8,11,13]. However there is no "visible" peak in the CDF data for R_{jj} close to 1. The contribution from other channels (called "central inelastic" in [2]) is too large and matches with the expected peak smoothly[3].

An alternative possibility is to measure exclusive $\gamma\gamma$ production with high $E_{\rm T}$ photons, $p\bar{p} \to p + \gamma\gamma + \bar{p}$ [2, 15]. Here there are no problems with hadronisation or with the identification of the jets. Moreover, we can access much higher masses of the centrally produced system than in the χ_c case. On the other hand the exclusive cross section is rather small. As usual, the perturbative QCD pomeron is described by two (Reggeized) gluon exchange. However the photons cannot be emitted from the gluon lines directly. We need first to create quarks. Thus a quark loop is required (see Fig. 2a), which causes an extra coupling $\alpha_{\rm s}(E_{\rm T})$ in the amplitude. The prediction of the cross section for exclusive $\gamma\gamma$ production, and the possible background contributions, are the subject of this paper.

In order to isolate the component of exclusive $\gamma\gamma$ production which is driven by two-gluon t-channel exchange, we need to consider other possible sources of these events. The possibilities are
(i) inclusive reactions in which the production of a $q\bar{q}$ pair is such that the quarks transfer almost the whole of their energy to the emitted photons (Fig. 2b), so that any additional hadrons (coming from the hadronisation of the q and $\bar{q}$) are soft, and so may be missed by the Central Detector;
(ii) diagrams with the t-channel quark exchange (Fig. 2c). We would expect this contribution to be suppressed at high energies. The quark densities generated from the incoming valence quarks in a fixed-order graph like Fig. 2c behave as $x_i q(x_i) \sim x_i$, whereas the gluons generated by the fixed-order diagram of Fig. 2a have distributions that behave as $x_i g(x_i) \sim$ constant, modulo $\log(x_i)$ factors. However the parton distributions at low x and moderate scales indicate that the quark densities are comparable to that of the gluon. On the other hand, the photons can be emitted directly from a quark line (without an extra loop and its accompanying small $\alpha_{\rm s}$ factor). Moreover the "skewed" factor, R_q, due to the asymmetric $q\bar{q}$ t-channel configurations is much larger for quarks, $R_q \sim 3$–4.5, than the corresponding factor for skewed t-channel gluons [16]. Since the exclusive cross section is proportional to R_q^4 [1], this is clearly important.

2 Exclusive $\gamma\gamma$ production via gg t-channel exchange

First, we calculate exclusive $\gamma\gamma$ production arising from gluon exchange, as shown in Fig. 2a. We write the cross section in the factorized form [2]

$$\sigma_g = \mathcal{L}_g(M^2_{\gamma\gamma}, y)\hat{\sigma}_g(M^2_{\gamma\gamma})\,, \quad (3)$$

where $\hat{\sigma}_g$ is the cross section for the hard $gg \to \gamma\gamma$ subprocess which produces a $\gamma\gamma$ system of mass $M_{\gamma\gamma}$, and $\mathcal{L}_g$ is the effective gg luminosity for production of a central system ($\gamma\gamma$ in our case) with rapidity y. For the exclusive $\gamma\gamma$ production shown in Fig. 2a we have, to single log accuracy [1],

$$M^2_{\gamma\gamma}\frac{\partial \mathcal{L}_g}{\partial y \partial M^2_{\gamma\gamma}} = \hat{S_g}^2 \left(\frac{\pi}{(N_C^2-1)b} \times \int \frac{{\rm d}q_{\rm t}^2}{q_{\rm t}^4} f_g(x_1, x_1', q_{\rm t}^2, \mu^2) f_g(x_2, x_2', q_{\rm t}^2, \mu^2)\right)^2, \quad (4)$$

where b is the t-slope corresponding to the momentum transfer distributions of the colliding proton and antiproton

$$\frac{{\rm d}^2\sigma}{{\rm d}t_1 {\rm d}t_2} \propto {\rm e}^{b(t_1+t_2)}\,. \quad (5)$$

We take $b = 4\,{\rm GeV}^{-2}$. The quantities $f_g(x, x', q_{\rm t}^2, \mu^2)$ are the generalised (skewed) unintegrated gluon densities. The skewed effect arises because the screening gluon (q) carries a much smaller momentum fraction $x' \ll x$. For small $|x - x'|$ the skewed unintegrated density can be calculated from the conventional integrated gluon $g(x, q_{\rm t}^2)$ [17]. However the full prescription is rather complicated. For this reason it is often convenient to use the simplified form [1]

$$f_g(x, x', q_{\rm t}^2, \mu^2) = R_g \frac{\partial}{\partial \ln q_{\rm t}^2}\left[\sqrt{T_g(q_{\rm t}, \mu)}\, x g(x, q_{\rm t}^2)\right], \quad (6)$$

[3] We hope that applying the $k_{\rm t}$ jet-searching algorithm, rather than the jet cone algorithm, would improve the selection of the exclusive events. This is in accord with the studies in [14].

which holds to 10–20% accuracy.[4] The factor R_g accounts for the single log q^2 skewed effect [16]. It is found to be about 1.4 at the Tevatron energy. The Sudakov factor $T_g(q_t, \mu)$ [18, 19] is the survival probability that a gluon with transverse momentum q_t does not emit any partons in the evolution up to the hard scale $\mu = M_{\gamma\gamma}/2$

$$T_g(q_t,\mu) = \exp\left(-\int_{q_t^2}^{\mu^2} \frac{\alpha_S(k_t^2)}{2\pi}\frac{dk_t^2}{k_t^2} \times \int_0^1 \left[\Theta(1-z-\Delta)\Theta(z-\Delta) z P_{gg}(z) + \sum_q P_{qg}(z)\right] dz\right), \quad (7)$$

with $\Delta = k_t/(\mu + k_t)$. The square root arises in (6) because the survival probability is only relevant to the hard gluon. It is the presence of this Sudakov factor which makes the integration in (4) infrared stable and perturbative QCD applicable. We use the MRST99 partons [20] and cut the loop integral at $q_t \geq 0.85\,\text{GeV}$, as in [5].

We also have to compute the probability $\hat{S}_g^{\,2}$ that the rapidity gaps are not populated by secondaries from soft rescattering from the colliding proton and antiproton. We calculate $\hat{S}_g^{\,2}$ using a two-channel eikonal model [21].

To compute the subprocess cross section, $\hat{\sigma}$, we use the known QED results for the $\gamma\gamma \to \gamma\gamma$ helicity amplitudes from [22,23]. Note that the incoming active gluons are in a P-even, $J_z = 0$ state [2,4,12], where z is the proton beam direction. Thus we need to compute the $J_z = 0$ $gg \to \gamma\gamma$ cross section, rather than the usual cross section averaged over the gluon polarisations. The results are shown in Fig. 3 for *fixed* $M_{\gamma\gamma} = 10\,\text{GeV}$ (continuous curve) and for *fixed* $E_{T\gamma} = 5\,\text{GeV}$ (dashed curve). All four flavours of quark (u, d, s, c) in the fermion loop were taken to be massless. The vertical dotted lines indicate the angles corresponding to a rapidity difference between the two photons $\eta_1 - \eta_2 = 1, 2$ or 3. We see that the logarithmic enhancement of the differential cross section at $|\cos\theta| \to 1$ for fixed $M_{\gamma\gamma}$ is strongly suppressed, by the Jacobian, when we select events with fixed $E_{T\gamma}$. The cross section decreases, since the fixed value of $E_{T\gamma}$ can only be achieved at small angles by increasing the value of $M_{\gamma\gamma}$, while the cross section behaves as $d\sigma/d\cos\theta \sim 1/M_{\gamma\gamma}^2$. Finally, combining the effective luminosity with the subprocess cross section, we obtain the predictions for the exclusive $\gamma\gamma$ cross section which we present and discuss in Sect 4.

There may be some contribution from the semi-elastic reaction with forward proton dissociation. Such a contribution was discussed in [5] for exclusive χ production. Provided the mass of the centrally produced system is not too large, it was argued that this contribution is small.[5] Moreover, the CDF measurement selects events without any

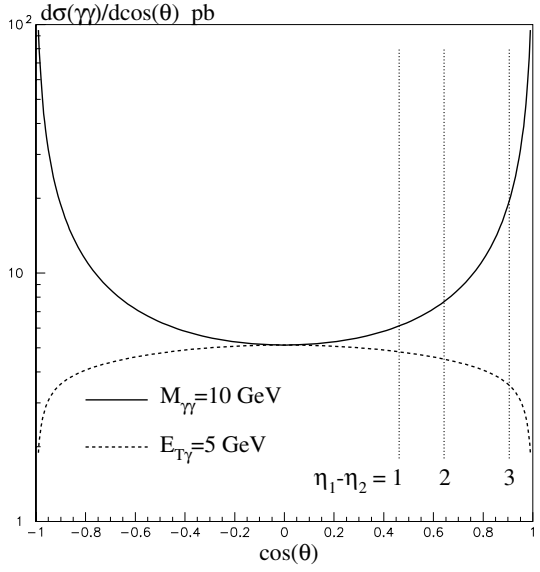

Fig. 3. The behaviour of the differential cross section for the $J_z = 0$ hard subprocess $gg \to \gamma\gamma$ in exclusive $\gamma\gamma$ production, shown by the continuous curve for fixed $M_{\gamma\gamma} = 10\,\text{GeV}$ and by the dashed curve for fixed $E_{T\gamma} = 5\,\text{GeV}$. The values of $\cos\theta$ corresponding to the rapidity differences of the two emitted photons $\eta_1 - \eta_2 = 1, 2$ or 3 are indicated

secondaries in the pseudorapidity interval $3.5 < |\eta| < 7.5$. This selection strongly suppresses the possibility of forward proton dissociation, and the admixture of processes with incoming proton dissociation is not expected to exceed 0.1%.

The background from the inclusive $q\bar{q}$ plus $\gamma\gamma$ production process, shown in Fig. 2b, may be estimated using the POMWIG Monte Carlo programme [25,26]. It is not anticipated to be large. For $E_T > 12\,\text{GeV}$ photons, the whole cross section in the rapidity interval $|\eta_\gamma| < 2$ ($\sim 100\,\text{fb}$) exceeds the exclusive cross section (Fig. 2a) by a factor of about 50. However the probability not to observe any hadrons produced via $q\bar{q}$ hadronisation is very small, so we hope that this background can be suppressed sufficiently to see the exclusive signal.

3 Exclusive $\gamma\gamma$ production via $q\bar{q}$ t-channel exchange

Here we discuss the $q\bar{q}$ t-channel exchange contribution to exclusive $\gamma\gamma$ production, as shown in Fig. 2c. This contribution has some novel features and so we discuss its computation in detail.

At first sight it appears that the contributions of the $q\bar{q}$ exchange graphs, Fig. 2c, may be neglected immediately, since the amplitudes are suppressed by the power factor $1/s$ in comparison with the gg exchange graphs. To be more precise, the suppression is given by $x \sim exp(-\Delta\eta_{\text{gap}})$. However, as mentioned in the Introduction, we must take care.

[4] In the actual computations we use a more precise form as given by (26) of [17].

[5] This reflects the smallness of the triple-pomeron vertex (see, for example, [24]) in soft processes. For the Tevatron the yields of exclusive and inclusive events are expected to be comparable at $M \sim 15\,\text{GeV}$, when gaps $|\Delta\eta_{\text{gap}}| > 3$ are imposed in the inclusive case.

First, the amplitude for the main process, Fig. 2a, contains a factor of $\alpha_s(E_T)$ arising from the quark loop. Second the $q\bar{q}$-exchange contribution to the cross section is enhanced by the skewed effect, $R_q^4 \sim 200$ [16]. Third, at the relatively low scales (a few GeV^2), relevant for the exclusive production of a system of mass $M \sim 10$–$30\,\mathrm{GeV}$ at the Tevatron, the global (CTEQ [27], MRST [28]) parton analyses find valence-like gluons (xg decreases as $x \to 0$, contrary to naive perturbative QCD expectations) but pomeron-like unpolarised singlet quarks ($xq \sim x^{-\lambda}$ with $\lambda > 0$). For these reasons the $q\bar{q}$-exchange contribution, Fig. 2c, must be evaluated.

In analogy with the computation of the gluon-exchange contribution, (3), we write the quark contribution as the product of the quark luminosity factor, $\mathcal{L}_q$, and the hard subprocess cross section, $\hat{\sigma}(q\bar{q} \to \gamma\gamma)$:

$$\sigma_q = \mathcal{L}_q(M_{\gamma\gamma}^2, y)\hat{\sigma}_q(M_{\gamma\gamma}^2)\,. \tag{8}$$

We discuss the computation of these factors in turn.

3.1 $q\bar{q}$ luminosity

To determine the luminosity, we first consider the leading-order $q\bar{q}$ exchange diagram, Fig. 4a, in the high energy limit. Note that s-channel helicity conservation, $\lambda = \lambda'$, holds for this process [29, 30]. This may be seen from the Born graph, Fig. 4b, corresponding to the upper part of the diagram. Due to helicity conservation at each vertex, a fast incoming quark of $\lambda = +1/2$, say, produces a gluon with $J_z^g = +1$, which then creates a quark with $\lambda' = +1/2$. This property allows us to close the external lines in Fig. 4a, and to calculate the numerator of the amplitude as

$$\mathrm{Tr}[\not{p}_a\gamma_\mu\not{q}\gamma_\nu\not{p}_b\gamma_\nu\not{q}'\gamma_\mu] = 4\mathrm{Tr}[\not{p}_a\,\not{q}\,\not{p}_b\,\not{q}'] = 8sq_t^2\,. \tag{9}$$

Here we consider the forward amplitude with $p'_{at} = 0$, and therefore $q_t = q'_t$. Note that only the transverse component, q_t, survives, since any longitudinal component of q or q' "annihilates" with p_a or p_b in (9); see [29, 30] for details. That is the lowest-order luminosity amplitude averaged over the incoming quark polarisations and colour indices is[6]

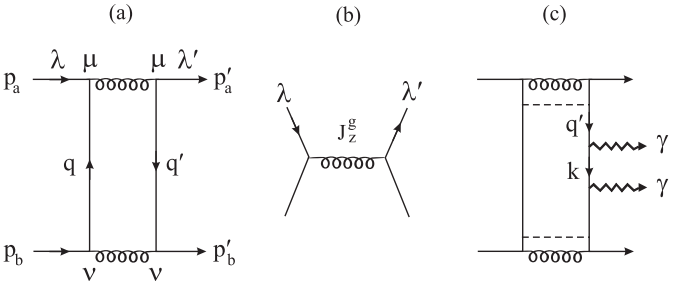

Fig. 4. **a** The LO $q\bar{q}$ exchange diagram; **b** the helicity structure of the upper part of diagram **a**; **c** the inclusion of the hard subprocess

[6] Here we consider the positive signature (singlet quark) exchange, where the real part of the amplitude is small, $|\mathrm{Re}\ A_q/\mathrm{Im}\ A_q| \ll 1$.

$$\mathrm{Im}\ A_q = \frac{16\pi^3}{N_C}\left(\frac{C_F}{2\pi}\alpha_s\right)^2\frac{\mathrm{d}q_t^2}{q_t^2}\,, \tag{10}$$

where $C_F\alpha_s/2\pi$ represents the lowest-order unintegrated quark distribution, given by the splitting function $P_{qq}(z)$ in the limit $z \to 0$. After evolution of the parton densities, each factor $C_F\alpha_s/2\pi$ should be replaced by the unintegrated distribution f_q/x. Now consider the inclusion of the hard subprocess, Fig. 4c, in which two photons of mass $M_{\gamma\gamma}$ are produced. The luminosity $\mathcal{L}_q$ in (8), corresponding to $q\bar{q}$ exchange with active quarks of a given flavour, is given by

$$\frac{\partial\mathcal{L}_q}{\partial y\partial\ln M_{\gamma\gamma}^2} = \hat{S}_q^2\left(\frac{2\pi}{N_C b}\int\frac{\mathrm{d}q_t^2}{q_t^2 M_{\gamma\gamma}^2}f_q(x_1,q_t^2,\mu^2)f_q(x_2,q_t^2,\mu^2)\right)^2\,. \tag{11}$$

The unintegrated quark distributions, f_q, are determined from the conventional quark densities by the relation

$$f_q(x,q_t^2,\mu^2) = R_q\frac{\partial}{\partial\ln q_t^2}\left(xq(x,q_t^2)\sqrt{T_q(q_t,\mu)}\right)\,, \tag{12}$$

in analogy with (6). Here the Sudakov factor is

$$T_q(q_t,\mu) = \exp\left(-\int_{q_t^2}^{\mu^2}\frac{\alpha_S(k_t^2)}{2\pi}\frac{\mathrm{d}k_t^2}{k_t^2}\int_0^{1-\Delta}P_{qq}(z)\mathrm{d}z\right)\,, \tag{13}$$

which ensures no gluon emissions in the quark evolution from q_t up to the hard scale μ. The q_t^2 in (9) is the reason why the $1/q_t^4$ in the analogous equation (4) becomes $1/q_t^2$ in (10) and in (11). The factor 2 in brackets reflects the fact that the hard subprocess may be initiated by either the t-channel quark with momentum q or q'. The origin of the $1/M_{\gamma\gamma}^2$ arises from the $1/s$ suppression of the $q\bar{q}$-exchange amplitude in comparison with the two-gluon-exchange amplitude, together with the $1/x_1x_2$ factors from the f_q/x noted above.

Strictly speaking the survival factor of the rapidity gaps, $\hat{S}_q^2$, in (11) may be different from the survival factor $\hat{S}_g^2$ in (4) for the gg exchange process, due to the different impact parameter profiles of the quarks and gluons inside the incoming protons [21, 31]. To account for the different profiles we may use different slopes b in (4) and (11). However it turns out [5] that for realistic values of $b = 4$–$6\,\mathrm{GeV}^{-2}$, the product $\hat{S}^2/b^2$ is almost constant. The value is $\hat{S}^2/b^2 = 3\times10^{-3}$ and $1.5\times10^{-3}\,\mathrm{GeV}^4$ for the Tevatron and the LHC respectively.

Another difference may arise since each eigenstate of the multichannel eikonal model, with its own absorptive cross section, may have its own parton composition [31]. However we do not expect this difference to be significant for low x partons.

3.2 The subprocess cross section

After the luminosity of (11) is calculated, the remainder of Fig. 4c, corresponding to the amplitude of the hard subprocess, contains the quark propagator $1/\not{k}$, the vertices of

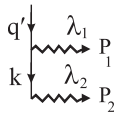

Fig. 5. The extra subamplitude we have to calculate for the $q\bar{q}$ subprocess for $\gamma\gamma$ production

the photon emissions, and an additional quark propagator, say $1/\not{q}'$, shown in the schematic diagram of Fig. 5. The structure of the subamplitude is of the form

$$\hat{\mathcal{M}}_{\lambda_1\lambda_2} = \frac{\not\epsilon_1 \not k_{(t)} \not\epsilon_2}{k^2_{(t)}} + \frac{\not\epsilon_2 \not k_{(u)} \not\epsilon_1}{k^2_{(u)}}, \tag{14}$$

where the additional quark propagator has been omitted for the moment. The two terms correspond to the t- and u-channel contributions, and so we have denoted the respective quark 4-momenta by $k_{(t)}$ and $k_{(u)}$. The diagrams of Fig. 4c and Fig. 5 show the t-channel contribution with $k \equiv k_{(t)}$, whereas the u-channel amplitude corresponds to the permutation of the two photons. Note that $k_{(t)} = q' - P_1$ and $k_{(u)} = q' - P_2$, where P_i are the momenta of the photons, $i = 1, 2$. For the photon helicities, we take the polarisation vectors

$$-{\epsilon_1}^{\pm},\ {\epsilon_2}^{\mp} = \mathrm{i}(\pm x' + \mathrm{i}y')/\sqrt{2}, \tag{15}$$

where the x', y' plane is perpendicular to the photon momentum in the $\gamma\gamma$ rest frame. In the massless quark limit, the amplitudes $\hat{\mathcal{M}}_{++}$ and $\hat{\mathcal{M}}_{--}$ vanish (see, for example, [32]), and so we need only consider $\hat{\mathcal{M}}_{\pm\mp}$. Using $\not\epsilon_1^+ \not\epsilon_2^- = 0$, we find

$$\hat{\mathcal{M}}_{+-} = \not\epsilon_1\ 2(q'\cdot\epsilon_2)\left(\frac{1}{k^2_{(t)}} + \frac{1}{k^2_{(u)}}\right), \tag{16}$$

since $k_{(t)} = q' - P_1$ and $\epsilon_2 \cdot P_1 = 0$ in the $\gamma\gamma$ rest frame. Finally we have to convolute $\not\epsilon_1$ with the quark propagator $\not q'_{\rm t}/q'^2$, and so the spin structure of the subprocess amplitude for the diagram of Fig. 5 is given by

$$\mathcal{M}_{+-} = 2(q'_{\rm t}\cdot\epsilon_1)(q'\cdot\epsilon_2)\left(\frac{1}{k^2_{(t)}} + \frac{1}{k^2_{(u)}}\right)\left(\frac{1}{q'^2}\right). \tag{17}$$

From the formal point of view, the result (17) may be regarded as the on-mass-shell amplitude for $q\bar{q} \to \gamma\gamma$ annihilation averaged over the quark colours and helicities, together with a specific averaging over the transverse momentum, $q'_{\rm t}$, of the incoming quark, which we specify below. We now justify this statement. First, at LO, $q'_{\rm t}$ in (11) is much less than the photon transverse momenta $P_{\rm t}$. In this limit the incoming quarks may be treated as on-mass-shell fermions. Second, the colour factor was already included in the colour singlet luminosity (11), so we must average over the colours of the quarks. Next, we have used unpolarised quark densities, so we need to average over the helicities of the quarks. The final "averaging" over $q'_{\rm t}$ is more subtle. Recall that in the calculation of the luminosity amplitude (10), only the transverse momentum component $q_{\rm t}$ survives in the t-channel quark propagator. (This is not the case for the usual on-mass-shell $q\bar{q} \to \gamma\gamma$ amplitude.) As a consequence of s-channel helicity conservation for the incoming proton, the projection of the total angular momentum of the produced $\gamma\gamma$ system on the beam (z) axis satisfies $J_z^{\gamma\gamma} = 0$. Recall that we are considering forward proton scattering. On the other hand, due to quark helicity conservation, we have $J_z^{q\bar{q}} = \pm 1$. So we require quark orbital angular momentum to satisfy $L_z = \pm 1$, which reveals itself through $q'_{\rm t}$. In the limit $q'_{\rm t} \to 0$, there is no way to generate $|L_z| = 1$. Angular momentum conservation kills everything which does not depend on $q'_{\rm t}$. Therefore the effective amplitude should be written as a difference of two matrix elements which correspond to subprocesses with different quark beam directions originating from their transverse momenta. This leads to

$$\frac{1}{N_C}\sum_{i,k}\delta_{ik}\ \frac{1}{2}\sum_{\lambda,\lambda'}\delta^{\lambda,-\lambda'}\ \frac{1}{2}\left[\mathcal{M}^{\lambda\lambda'}_{ik}(q'_{\rm t}) - \mathcal{M}^{\lambda\lambda'}_{ik}(-q'_{\rm t})\right], \tag{18}$$

where i, k and λ, λ' are the quark colour and helicity indices respectively. For simplicity, elsewhere in the paper these indices have been omitted. At first sight, this expression still appears to vanish once we integrate over the azimuthal angle of $q'_{\rm t}$. Indeed this is true for a point-like amplitude $\mathcal{M}$; for example for forward central exclusive production of a Z boson. However for our non-local amplitude, there is a correlation between the direction of the quark $q'_{\rm t}$ and the photon $P_{\rm t}$. Thus a contribution of $O(q'^2_{\rm t}/P^2_{\rm t})$ survives after the azimuthal angular averaging of $(q'_{\rm t}\cdot\epsilon_1)(q'\cdot\epsilon_2)$ in (17). This $q'^2_{\rm t}$ cancels the factor $1/q'^2 \simeq 1/q'^2_{\rm t}$ in (17), coming from the quark propagator, and so finally we obtain the effective $q\bar{q} \to gg$ hard subprocess cross section[7]

$$\frac{{\rm d}\hat{\sigma}_{\rm eff}}{{\rm d}t} = 16\pi\left(\frac{e_q^2\alpha}{M^2_{\gamma\gamma}}\right)^2\left(\frac{\cos\theta}{\sin\theta}\right)^4. \tag{19}$$

[7] The behaviour ${\rm d}\hat{\sigma}/{\rm d}t \propto (1/M^4_{\gamma\gamma})(\cos\theta/\sin\theta)^4$ may be explained without an explicit calculation, instead using arguments based on the rotation properties of the amplitude and the Wigner d-functions. Indeed, for spinless particles, ${\rm d}\sigma/{\rm d}t \propto r_T^4$, where the radius of interaction $r_{\rm T} \sim 1/P_{t\gamma} \sim 1/\sin\theta$. This is easy to check in $\lambda\phi^3$ theory. Next we have to satisfy a set of selection rules. We consider the photon helicity amplitude with $(\lambda_1, \lambda_2) = (+,-)$ (or $(-,+)$), which has projection $|J_{z'}| = 2$ of the total $\gamma\gamma$ angular momentum on the photon axis z'. Simultaneously the projection of the total $\gamma\gamma$ angular momentum on the quark axis, z_q, is $J_{z_q} = \pm 1$. The probability amplitude for such a configuration is given by $\sin\theta\cos\theta$. On the other hand the projection on the incoming proton direction (z) is $J_z = 0$. This can only be possible due to the precession of the quark axis z_q around the proton axis z with $|L_z| = 1$. The probability amplitude to have $|L_z| = 1$ is proportional to $q_{\rm t} r_{\rm T}$, that is to the ratio of the quark and photon transverse momenta $q_{\rm t}/P_{t\gamma} \sim 1/\sin\theta$. Finally we need to take the right sign of L_z, and to sum the contribution of the "t" and "u" channel diagrams. Since the "u" channel is obtained by replacing $P_{\rm t}$ by $-P_{\rm t}$, this gives another factor $\cos\theta$ (as in the difference of the two d-functions $d^1_{1,1} - d^1_{1,-1} = \cos\theta$). Thus we obtain an additional factor in the amplitude of $(\cos\theta/\sin\theta)\sin\theta\cos\theta = \cos^2\theta$. The behaviour ${\rm d}\hat{\sigma}/{\rm d}t \propto 1/M^4_{\gamma\gamma}$ comes just from dimensional counting. Therefore, including the first kinematical factor of $1/\sin^4\theta$, we obtain ${\rm d}\hat{\sigma}/{\rm d}t \propto (1/M^4_{\gamma\gamma})\ (\cos\theta/\sin\theta)^4$.

Here e_q is the electric charge of the quark and θ is the scattering angle in the $\gamma\gamma$ rest frame.

To calculate the observable cross section we have to include the contributions of the active quarks and antiquarks of all flavours. However the luminosity (11) is written for the cross section for one type of quark. To sum up all the quark contributions we must sum the $q\bar{q}$ luminosity amplitudes (given by the square root of the right hand side of (11)) multiplied by the amplitudes of the hard subprocess (and not the cross sections). Finally we have accounted for the identity of the photons and summed over the $(+,-)$ and $(-,+)$ photon helicity configurations in the cross section.

4 Discussion of results

Using the formalism described above, we have calculated the cross section of exclusive $\gamma\gamma$ production for the Tevatron ($\sqrt{s} = 1.96\,\text{TeV}$) and the LHC energy ($\sqrt{s} = 14\,\text{TeV}$). In Fig. 6 we present the cross section integrated over the kinematic domain in which the emitted photons have transverse energy $E_\text{T} > E_\text{cut}$ and centre of mass rapidity, for both photons, either $|\eta_\gamma| < 1$ or $|\eta_\gamma| < 2$. Clearly the dominant contribution comes from gg t-channel exchange. In spite of the large enhancement coming from the skewed quark factor, $R_q^4 \sim 200$, the contribution which originates from $q\bar{q}$ exchange is more than two orders of magnitude lower; and it falls more steeply with increasing E_T due to the factor $1/M_{\gamma\gamma}^4$ in the luminosity. Such a small $q\bar{q}$ exchange contribution to exclusive $\gamma\gamma$ production is explained, first, by the $(q_\text{t}'^2/M_{\gamma\gamma}^2)$ suppression coming from angular momentum conservation, and, secondly, by the $\cos^4\theta$ behaviour of the subprocess cross section. The cross section vanishes at 90 degrees, while the η_γ cuts select events with small $\cos\theta$. Calculating the interference between the gg and $q\bar{q}$ exchange amplitudes, we account for the helicity structure of the hard subprocess amplitudes and for the complex phase of the $gg \to \gamma\gamma$ amplitude.

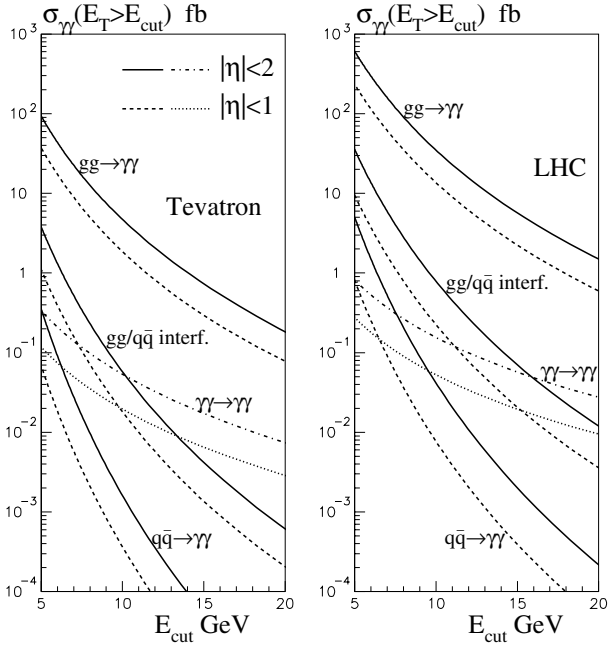

Fig. 6. The contributions to the cross section for exclusive $\gamma\gamma$ production from gg and $q\bar{q}$ exchange at the Tevatron and the LHC. Also shown is the contribution from the QED subprocess $\gamma\gamma \to \gamma\gamma$. For each component we show the cross section restricting the emitted photons to have $E_\text{T} > E_\text{cut}$ and to lie in the centre of mass rapidity interval $|\eta_\gamma| < 1$ (or $|\eta_\gamma| < 2$)

The results shown in Fig. 6 are obtained using MRST partons [20]. The predictions differ by up to about 20% if CTEQ partons [27] are used; the cross section being a little larger at the Tevatron and a little smaller at the LHC.

Recall that both the luminosities $\mathcal{L}_g$ and $\mathcal{L}_q$ were calculated for forward outgoing protons, that is in the limit of vanishing p'_{at} and p'_{bt}. This is a very good approximation for the $q\bar{q}$-exchange contribution, since the additional suppression factor $(q_\text{t}'^2/M_{\gamma\gamma}^2)$, which is implicit in (11), in comparison with (4), makes the q_t integral logarithmic. In addition, the Sudakov factor T_q in (12) pushes the dominant q_t^2 region, in the integral, closer to the factorisation scale μ^2. This justifies the use of the massless quark approximation to calculate the effective cross section (19). Since the colour charge of the quark is smaller than that of the gluon, and the dominant q_t^2 interval is closer to μ^2, the suppression of the $q\bar{q}$-exchange contribution of the cross section arising from T_q (~ 0.6–0.8) is much weaker than the suppression of the gg-exchange component due to T_g.

The corrections due to non-zero p'_{it} of the outgoing protons, which are the order of $(p'_{it}/q_\text{t})^2 \sim 1/q_\text{t}^2 b$, are quite small. For the gg-exchange contribution, the saddle point of the integral (4) is in the region $q_\text{t}^2 \sim 1$–$1.5\,\text{GeV}^2$ for the Tevatron energy, and $q_\text{t}^2 \sim 1.5$–$3\,\text{GeV}^2$ for the LHC energy, depending on the value of E_T. Thus the violation of the $J_z = 0$ selection rule may be as large as $(p_{it}'^2/q_\text{t}^2)^2 \sim 10\%$.

It is interesting to note that the fraction of $q\bar{q}$ induced events at the LHC is larger than that at the Tevatron. This is because the quark densities at relatively large scales grow faster, with decreasing x, than the gluon densities at lower scales and low x.

To complete the discussion of the sources of exclusive $\gamma\gamma$ events we consider contributions originating from large-distance processes. First we have the QED process shown in Fig. 7a. The effective $\gamma\gamma$ luminosity reads

$$\frac{\partial\mathcal{L}_{\gamma\gamma}}{\partial y\partial\ln M_{\gamma\gamma}^2} = \hat{S}_\gamma^2 \left(\frac{\alpha}{\pi}\right)^2 \int_{q_\text{min}^2} \frac{\mathrm{d}q_1^2}{q_1^2} F_N^2(q_1^2) \int_{q_\text{min}^2} \frac{\mathrm{d}q_2^2}{q_2^2} F_N^2(q_2^2)\,, \tag{20}$$

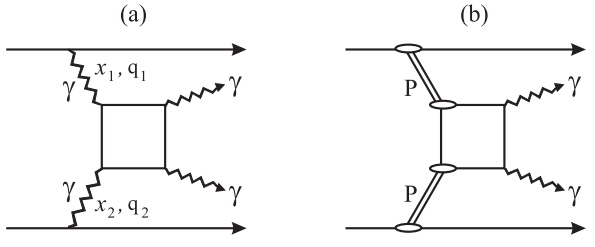

Fig. 7. Large-distance contributions to exclusive $\gamma\gamma$ production: **a** the QED induced process, and **b** the pomeron–pomeron fusion process

with $q^2_{\min,i} = x_i^2 m_p^2$, where m_p is the mass of the proton. The momentum fractions carried by the incoming photons are

$$x_{1,2} = (M_{\gamma\gamma}/\sqrt{s})\mathrm{e}^{\pm y}\,. \tag{21}$$

The F_N are the usual dipole form factors of the proton. They provide the upper cut-off on the integrals. To calculate the $\gamma\gamma \to \gamma\gamma$ amplitudes we use [22, 23]. We include fermion loops for the quarks, electron, muon and tau. Since the $\gamma\gamma$ luminosity comes from large impact parameters, that is very low q_i^2, the survival factor $\hat{S}^2_\gamma \sim 1$; see [33]. The resulting exclusive QED contribution to the $\gamma\gamma$ cross section is shown in Fig. 6[8].

Next we consider the same process but with the t-channel photons replaced by pomerons; see Fig. 7b. We use this diagram to compute the low q_t ($< 0.85\,\mathrm{GeV}$) contribution to the luminosity in (4), which was excluded from the perturbative calculation. We put the same limit on the virtuality of the t-channel left quark line in Fig. 7b. This cut-off strongly reduces the size of the pomeron–pomeron $\to \gamma\gamma$ amplitude. Unlike exclusive χ_c production, where the perturbative and non-perturbative contributions are comparable [5], here the $\gamma\gamma$ yield from Fig. 7b is less than a few percent of the perturbative $gg \to \gamma\gamma$ cross section. As noted in [5], there is no interference between the real amplitudes of the diagrams in Fig. 7 and the imaginary amplitude corresponding to Fig. 2a; here we refer to the luminosity amplitudes, since for the $J_z = 0$ case the fermion loop contribution is real. Strictly speaking this is only true for the process Fig. 7b if we assume that the non-perturbative pomeron interacts with the quark via a photon-like vertex γ_μ, which provides s-channel quark helicity conservation. For the case of γ-exchange, Fig. 7a, there may be some $|J_z| = 2$ contribution where the $\gamma\gamma \to \gamma\gamma$ amplitude has its own imaginary part. However this contribution, coming from large impact parameters b_t, corresponds to very low p_{it} of the forward protons and thus essentially does not interfere with the main amplitude, Fig. 2a.

5 Conclusions

The double-diffractive exclusive production of a massive system (such as a Higgs boson) is a good way to search, and to study, new physics at the LHC. The existence of rapidity gaps on either side of the system means that the event rate will be suppressed. The observation of the exclusive production of a pair of high E_T photons at the Tevatron offers the possibility to check the exclusive prediction of these types of process. As can be seen from Fig. 6, the dominant contribution to the exclusive diffractive production of such a pair of photons is driven by the same two-gluon-exchange mechanism, that is by the same effective gg luminosity, $\mathcal{L}_g$, as is exclusive diffractive Higgs boson production. Therefore, indeed, this process can be used as a "standard candle" to check and to monitor the exclusive gg luminosity, $\mathcal{L}_g$, that has been used for the prediction of the Higgs cross section.

The uncertainty of the predictions comes from the parton distributions used to calculate the luminosities, the model dependent calculation of the survival factors $\hat{S}^2$ and the lack of knowledge of the NLO corrections to the hard subprocess. The first two have been discussed above and in [34]. Since we would like to use exclusive $\gamma\gamma$ as a "standard candle" to monitor the exclusive gg luminosity, $\mathcal{L}_g$, it is important to calculate the NLO correction to $gg \to \gamma\gamma$ amplitudes accounting for the presence of the additional t-channel gluon (shown on the left in Fig. 2a) which provides the effective infrared cut-off for the NLO loop contribution.

Acknowledgements. We thank Mike Albrow, Albert De Roeck, Risto Orava, and especially Beate Heinemann and Angela Wyatt for useful discussions and encouragement. ADM thanks the Leverhulme Trust for an Emeritus Fellowship and MGR thanks the IPPP at the University of Durham for hospitality. This work was supported by the UK Particle Physics and Astronomy Research Council, by a Royal Society special project grant with the FSU, by grant RFBR 04-02-16073 and by the Federal Program of the Russian Ministry of Industry, Science and Technology SS-1124.2003.2.

[8] For large E_T, $E_\mathrm{T} > 110\,\mathrm{GeV}$, the QED contribution starts to dominate. However the cross section is very small, about 3×10^{-4} fb for $|\eta_\gamma| < 2$ at the LHC.

References

1. V.A. Khoze, A.D. Martin, M.G. Ryskin, Eur. Phys. J. C **14**, 525 (2000)
2. V.A. Khoze, A.D. Martin, M.G. Ryskin, Eur. Phys. J. C **23**, 311 (2002)
3. A.B. Kaidalov, V.A. Khoze, A.D. Martin, M.G. Ryskin, Eur. Phys. J. C **33**, 261 (2004)
4. V.A. Khoze, A.D. Martin, M.G. Ryskin, Eur. Phys. J. C **19**, 477 (2001), Erratum C **20**, 599 (2001)
5. V.A. Khoze, A.D. Martin, M.G. Ryskin, W.J. Stirling, Eur. Phys. J. C **35**, 211 (2004)
6. A.D. Martin, M.G. Ryskin, V.A. Khoze, Phys. Rev. D **56**, 5867 (1997)
7. A. De Roeck, V.A. Khoze, A.D. Martin, R. Orava, M.G. Ryskin, Eur. Phys. J. C **25**, 391 (2002)
8. M. Gallinaro (representing the CDF Collaboration), FERMILAB- CONF-03-403-E, November 2003, hep-ph/0311192
9. WA102 Collaboration: D. Barberis et al., Phys. Lett. B **467**, 165 (1999); B **474**, 423 (2000); B **484**, 198 (2000); B **488**, 225 (2000); B **453**, 305, 316 (1999)
10. V.A. Khoze, A.D. Martin, M.G. Ryskin, Eur. Phys. J. C **24**, 581 (2002)
11. K. Goulianos (representing the CDF collaboration), FERMILAB-CONF-03-277-E, AIP Conf. Proc. **698**, 110 (2004), hep-ph/0308183
12. V.A. Khoze, A.D. Martin, M.G. Ryskin, hep-ph/0006005, in Proceedings of 8th International Workshop on Deep Inelastic Scattering and QCD (DIS2000), Liverpool, edited by J. Gracey, T. Greenshaw (World Scientific, 2001), p. 592; V.A. Khoze, A.D. Martin, M.G. Ryskin, Nucl. Phys. Proc. Suppl. B **99**, 188 (2001)
13. CDF Collaboration: T. Affolder et al., Phys. Rev. Lett. **85**, 4215 (2000)

14. B. Cox, J.R. Forshaw, A. Pilkington, in preparation
15. M. Albrow, A. Rostovtsev, hep-ph/0009336
16. A.G. Shuvaev, K.J. Golec-Biernat, A.D. Martin, M.G. Ryskin, Phys. Rev. D **60**, 014015 (1999)
17. A.D. Martin, M.G. Ryskin, Phys. Rev. D **64**, 094017 (2001)
18. M.A. Kimber, A.D. Martin, M.G. Ryskin, Phys. Rev. D **63**, 114027 (2001)
19. G. Watt, A.D. Martin, M.G. Ryskin, Eur. Phys. J. C **31**, 73 (2003)
20. A.D. Martin, R.G. Roberts, W.J. Stirling, R.S. Thorne, Eur. Phys. J. C **14**, 133 (2000)
21. V.A. Khoze, A.D. Martin, M.G. Ryskin, Eur. Phys. J. C **18**, 167 (2000)
22. A.I. Akhiezer, Phys. Z. Sowjetunion **11**, 263 (1937); R. Karplus, M. Neumann, Phys. Rev. **80**, 380 (1950); **83**, 776 (1957); B. De Tollis, Nuovo Cimento, **32**, 757 (1964); **35**, 1182 (1965)
23. Z. Bern, A. De Freitas, L. Dixon, A. Ghinculov, H.L. Wong, JHEP **0111**, 031 (2001)
24. A.B. Kaidalov, V.A. Khoze, Yu.F. Pirogov, N.L. Ter-Isaakyan, Phys. Lett. B **45**, 493 (1973); A.B. Kaidalov, K.A. Ter-Martirosyan, Nucl. Phys. B **75**, 471 (1974); A.B. Kaidalov, Phys. Rept. **50**, 157 (1979)
25. POMWIG: B. Cox, J. Forshaw, Comput. Phys. Commun. **144**, 104 (2002)
26. B. Cox, J. Forshaw, B. Heinemann, Phys. Lett. B **540**, 263 (2002)
27. CTEQ Collaboration: J. Pumplin et al., JHEP **0207**, 012 (2002)
28. A.D. Martin, R.G. Roberts, W.J. Stirling, R.S. Thorne, Eur. Phys. J. C **28**, 455 (2003)
29. V.G. Gorshkov, V.N. Gribov, L.N. Lipatov, V.G. Frolov, Sov. J. Nucl. Phys. **6**, 95 (1967)
30. R. Kirschner, L.N. Lipatov, Nucl. Phys. B **213**, 122 (1983)
31. A.B. Kaidalov, V.A. Khoze, A.D. Martin, M.G. Ryskin, Eur. Phys. J. C **21**, 521 (2001)
32. V.S. Fadin, V.A. Khoze, A.D. Martin, Phys. Rev. D **56**, 484 (1997)
33. V.A. Khoze, A.D. Martin, M.G. Ryskin, Eur. Phys. J. C **24**, 459 (2002)
34. A.B. Kaidalov, V.A. Khoze, A.D. Martin, M.G. Ryskin, Eur. Phys. J. C **31**, 387 (2003)